POTENTIAL CLINICAL SIGNIFICANCE

Nanomedicine: Nanotechnology, Biology, and Medicine
12 (2016) 871–879

Original Article

nanomedjournal.com

Development of a complementary PET/MR dual-modal imaging probe for targeting prostate-specific membrane antigen (PSMA)

Sung-Hyun Moon, MS[a,b], Bo Yeun Yang, PhD[a], Young Ju Kim, BS[a,c], Mee Kyung Hong, MS[a,c], Yun-Sang Lee, PhD[a], Dong Soo Lee, MD, PhD[a], June-Key Chung, MD, PhD[a,b,c], Jae Min Jeong, PhD[a,b,c,*]

[a]*Department of Nuclear Medicine and Institute of Radiation Medicine, Seoul National University College of Medicine, Seoul, Korea*
[b]*Department of Radiation Applied Life Science, Seoul National University College of Medicine, Seoul, Korea*
[c]*Cancer Research Institute, Seoul National University College of Medicine, Seoul, Korea*

Received 25 November 2015; accepted 9 December 2015

Abstract

We tried to develop a dual-modal PET/MR imaging probe using a straightforward one-pot method by encapsulation with specific amphiphiles. In this study, iron oxide (IO) nanoparticles were encapsulated with three amphiphiles containing PEG, DOTA and the prostate-specific membrane antigen (PSMA)-targeting ligand in aqueous medium. The diameter of the prepared nanoparticle DOTA-IO-GUL was 11.01 ± 1.54 nm. DOTA-IO-GUL was labeled with ^{68}Ga in high efficiency. The DOTA-IO-GUL showed a dose-dependent binding to LNCaP (PSMA positive) cells via a competitive binding study against ^{125}I-labeled MIP-1072 (PSMA-targeting agent). Additionally, PET and MR imaging results showed PSMA selective uptake by only 22Rv1 (PSMA positive) but not PC-3 (PSMA negative) in dual-tumor xenograft mouse model study. MR imaging showed high resolution, and PET imaging enabled quantification and confirmation of the specificity. In conclusion, we have successfully developed the specific PSMA-targeting IO nanoparticle, DOTA-IO-GUL, as a dual-modality probe for complementary PET/MR imaging.

From the Clinical Editor: The combination of using Positron Emission Tomography (PET) and computed tomography (CT) in clinical practice is now the norm. With advances in technology, the next step would be to develop combined PET and Magnetic Resonance (MR) dual-imaging. In this article, the authors described their positive study on the development of a dual-modal PET/MR imaging probe using a prostate cancer model.

Key words: Encapsulation; GUL; Prostate cancer; Multi-modal; Gallium-68

A combined system of positron emission tomography (PET) and magnetic resonance (MR) dual-imaging emerged as an important topic in nuclear medicine and molecular imaging studies.[1-6] PET/computed tomography (CT) was developed for its complementary effect of using both PET and CT imaging, which replaced most PET-only instruments. Because of the higher sensitivity and specificity of MR imaging compared with CT, PET/MR dual-imaging is expected to be the next generation of PET/CT.[7-12] Thus, the development of a probe for PET/MR dual-imaging is necessary for the implementation of this synergistic instrument. Recently, PET/MRI agents are produced by using various materials such as Gd, Cu, Zr, iron oxide, etc.[13-17] These PET/MRI agents are used for T1 or T2 imaging according to function and characteristics of each material.

Nanoparticles (NP) are widely studied for their use as imaging probes,[18,19] especially because they have a large surface area relative to volume or diameter, which allows them to introduce special ligands and multiple beacons for targeting and imaging.[20,21] Various surface modification methods have been investigated to produce multimodal imaging NPs, most of which included step-by-step modification using chemical reactions and purification. However, these methods have intrinsic drawbacks such as low yield and poor reproducibility.[22,23] A novel, straightforward encapsulation method producing high yield and high reproducibility has been reported[24-27]: in this method, NPs

Funding sources: National Research Foundation of Korea (NRF-2012M2A2A7035853 and NRF-2013R1A2A1A05006227).

Conflict of interest: No.

*Corresponding author at: Department of Nuclear Medicine and Institute of Radiation Medicine, Seoul National University College of Medicine, Seoul, Korea.
E-mail address: jmjng@snu.ac.kr (J.M. Jeong).

http://dx.doi.org/10.1016/j.nano.2015.12.368

are mixed and encapsulated with specially designed amphiphiles by vortexing, heating and sonication. This method could easily be applied to various kinds of NPs with hydrophobic surface, such as quantum dots, iron oxide, gold, etc.

Iron oxide (IO) NPs have been actively investigated as MRI contrast agents in clinical trials.[28-33] Furthermore, they have also been applied as PET/MR dual imaging probes after being labeled with positron emitters.[9,12,25,34]

^{68}Ga is a well-known positron emitter having an adequate half-life for diagnostic imaging (68 min), and is produced by a ^{68}Ge/^{68}Ga-generator which has huge economical and technical merits.[35,36] Bifunctional chelating agents are essential for labeling NPs with ^{68}Ga.[37-39] The 1,4,7,10-tetraazacyclododecane-1,4,7,10-tetraacetic acid (DOTA) is one of the most widely used bifunctional chelating agents.[40] Particularly, DOTA could be used for both diagnostic radioisotopes such as ^{68}Ga and ^{111}In, and therapeutic radioisotopes such as ^{90}Y and ^{177}Lu, which is important for the theranostic use of NPs.

Prostate cancer is one of the most common types of cancer in the world.[41,42] The prostate specific membrane antigen (PSMA) is a well-known biomarker of prostate cancer, therefore many PSMA targeting molecules have been developed and investigated.[43-48] Furthermore, the glutamate-urea-lysine (GUL) conjugate has been proven to be a PSMA targeting moiety and its 3D structure has also already been published.[49]

In this study, we aim to develop a new PSMA-targeting IO NP for use in PET/MR dual-imaging. To achieve this, we employed the encapsulation method using amphiphiles containing DOTA and GUL each conjugated with a long alkyl chain and commercially available IO NP. The DOTA moiety was used for labeling with ^{68}Ga and the GUL moiety was used for targeting PSMA. The IO core was used for MR imaging.

Methods

General remarks

Oleic acid-coated IO NP in chloroform was purchased from MKnano (MK Implex Corp., ON, Canada). The hydrodynamic diameter and size distribution of nanoparticles were analyzed using the DLS system from Zetasizer Nano ZS90 (Malvern Instruments Ltd., Worcestershire, UK) and transmission electron microscope (TEM) imaging using the JEM-1400 electron microscope (JEOL Ltd., Tokyo, Japan). A SCINCO S-3100 was used for UV/vis spectrometer (SCINCO America, WI, USA). The ^{68}Ge/^{68}Ga-generator was purchased from ITG (ITG GmbH, Munich, Germany). Instant thin layer chromatography-silica gel (ITLC-SG) was purchased from Agilent Technologies, Inc. (CA, USA). Radio-TLC was counted using a Bio-Scan AR-2000 System imaging scanner (Bioscan, WI, USA). Animal PET/CT imaging was performed using the eXplore Vista PET/CT scanner (GE Healthcare, CT, USA). Animal PET imaging was performed using the G4 PET X-RAY scanner (Sofie Biosciences, Culver City, CA, USA).The Agilent 9.4T 160/AS MRI system and millipede coil (both radiofrequency transmission and signal reception) (Agilent Technologies, Santa Clara, CA, USA) were used for the MRI system.

All animal studies were performed at the Seoul National University Hospital, Seoul, Korea, which is fully accredited by AAALAC International (2007, Association for Assessment and Accreditation of Laboratory Animal Care International).

Preparation of the DOTA-IO-GUL nanoparticle

The DOTA-SA (2.57 mg, 3.19 μmol) and GUL-SA (3.27 mg, 3.19 μmol) were suspended in a solution of 8% Tween® 60 in distilled water (v/v, 1 mL) in a 2-mL glass vial. The reaction mixture was sonicated for 30 min using the ultrasonicator (77.8 W, amplitude = 70%, cycle = 1). Then, IO in chloroform (5 mg/mL, 100 μL) was slowly added. The reaction mixture was sonicated for 10 min and heated to 80 °C for 10 min. This step was repeated 3 times to remove chloroform. After removing the chloroform, the reaction mixture was sonicated for 2 h (77.8 W, amplitude = 70%, cycle = 1). Finally the reaction mixture was changed to clear dark brown color solution. The reaction mixture was purified by Sephacryl® S-500 HR-packed column chromatography (14.5 × 150 mm, V_0 = 2.37 mL) using distilled water as an eluent. The clean brown fractions were collected and concentrated by ultrafiltration (Amicon Ultra-0.5, 100 kDa, 5000 G, 30 °C, 5 min).

Size analysis

DOTA-IO-GUL hydrodynamic diameter, size distribution and zeta potential were measured by the DLS instrument. Sample DOTA-IO-GUL (10 μL) was dissolved in distilled water (1 mL). This prepared sample was measured in a cuvette for DLS. The measured particle size and distribution were obtained in number-percent (%) value at 25 °C at a scattering angle of 90°. Zeta potential was also measured by the DLS.

TEM was used for shape examination and size confirmation. Samples were diluted 100 times using distilled water and were dropped into the Ni coated metal grid. TEM images were obtained using an acceleration voltage of 80 keV.

Ferric ion concentration analysis

The Fe concentration of encapsulated DOTA-IO-GUL was analyzed using the iron thiocyanate colorimetric method. This method was based on Beer's law plot of iron(III) thiocyanate absorbance at 481 nm. Various concentrations of $Fe(NO_3)_3$ standard (0.1, 0.08, 0.06, 0.04, and 0.02 M), 0.5 M nitric acid and 1 M potassium thiocyanate solutions were prepared. Each 5 μL aliquot of $Fe(NO_3)_3$ and sample DOTA-IO-GUL solution was mixed with 1 mL of 0.5 M nitric acid solution. The mixture was incubated for 30 min at room temperature, and then 1 mL of 1 M potassium thiocyanate was added to each mixture. After vortexing, the mixture was incubated for 30 min at room temperature. The absorbance of the resulting $Fe(SCN)^{2+}$ solution at 481 nm was measured by the UV–vis spectrophotometer. The standard equation of standard Fe^{3+} concentration versus absorbance at 481 nm was drawn from the data by linear regression. The Fe^{3+} concentration of DOTA-IO-GUL was obtained from the equation and the absorbance of the sample.

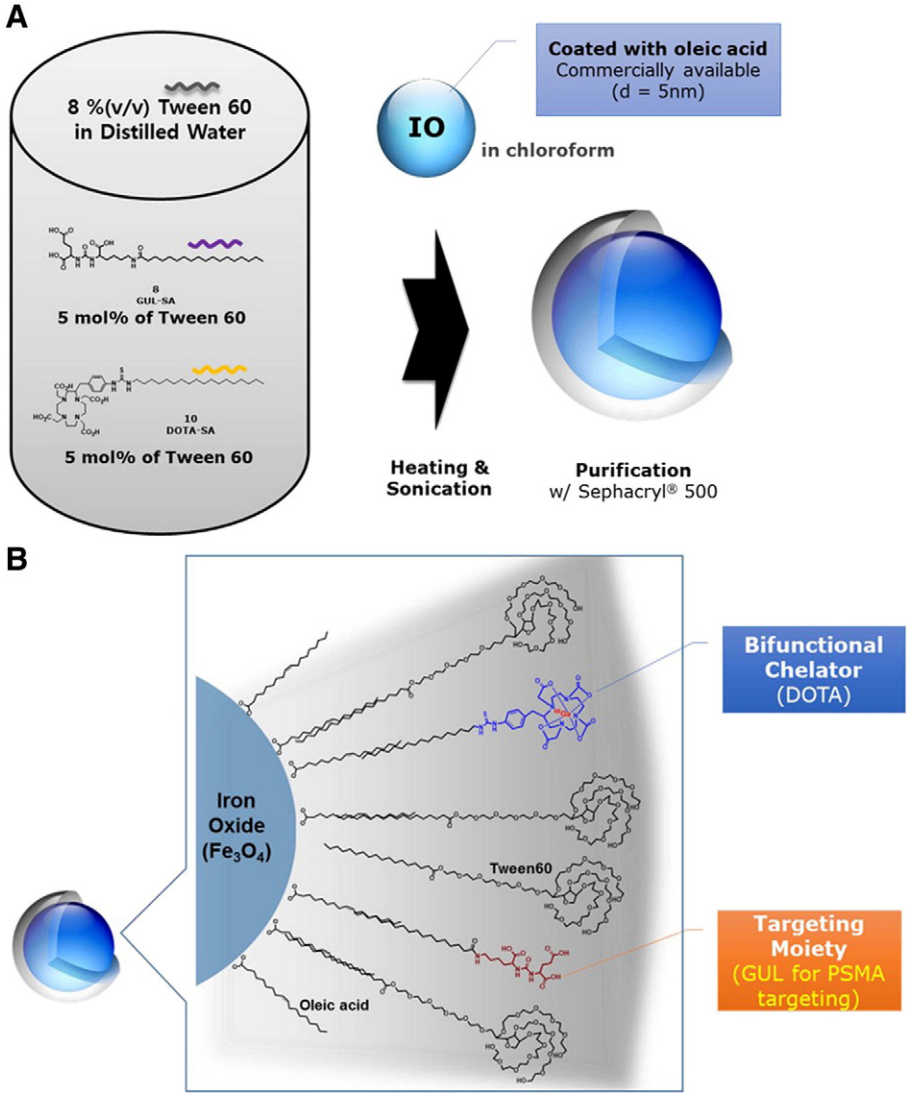

Figure 1. **(A)** Encapsulation of NPs with specific amphiphiles. **(B)** Diagram of encapsulated DOTA-IO-GUL.

Stability test in salt solution

The stability of DOTA-IO-GUL in a high salt solution was tested by the incubation of DOTA-IO-GUL in 0.9%, 1.8% and 3.6% NaCl (w/v) aqueous solution. These mixtures were incubated at room temperature and NP sizes were measured by DLS at 1 h, 12 h and 24 h.

^{68}Ga labeling

$^{68}GaCl_3$ (111 MBq) in 0.1 M HCl solution (200 μL) was added to 1 M sodium acetate buffer (pH = 5.6, 200 μL). DOTA-IO-GUL (20 μL) was added and vortexed for 1 min. The reaction mixture was incubated for 30 min at 90 °C and was then cooled to room temperature. The labeling efficiency of ^{68}Ga-DOTA-IO-GUL was measured by ITLC-SG eluted with 0.1 M citric acid and scanned by the radio-TLC scanner. The medium of ^{68}Ga-DOTA-IO-GUL solution was replaced with distilled water by centrifugal ultrafiltration (0.4 mL, 3 times) and concentrated to 100 μL using the Amicon tube by centrifugation.

Stability test in serum

^{68}Ga-DOTA-IO-GUL (3.7 MBq, 100 μL) was added to human serum (1 mL) and was then vortexed vigorously. The mixture was incubated in a shaking incubator at 37.5 °C. After 2 h, the radiochemical purity of the reaction mixture was tested by radio-TLC as described above. We also compared the gel filtration (Sephacryl® S-500 HR; column: 14.5 × 150 mm) elution profiles of ^{68}Ga-DOTA-IO-GUL before and after the incubation with human serum.

Human prostate cancer cell culture

Two PSMA-positive prostate cancer cell lines, 22Rv1 and LNCaP, and one PSMA-negative prostate cell line, PC-3, were used for this study. All prostate cancer cell lines were grown in a humidified incubator with a 5% carbon dioxide supply at 37 °C. The 22Rv1 cell line was purchased from ATCC and was grown in ATCC-formulated RPMI 1640 (WELGENE Inc., Korea) mixed with 10% (v/v) heat inactivated fetal bovine serum (FBS)

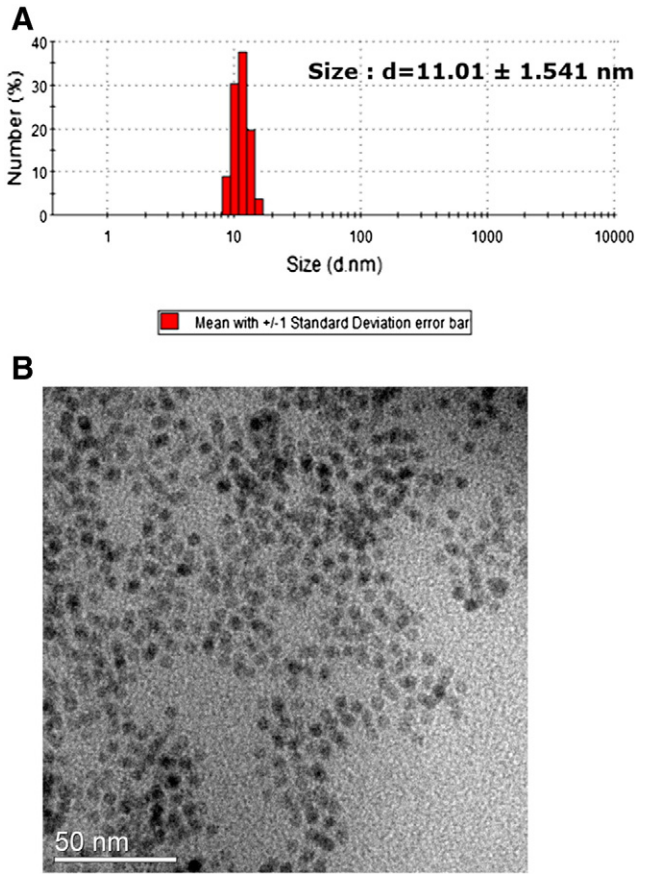

Figure 2. Size determination of DOTA-IO-GUL. **(A)** DLS data of DOTA-IO-GUL (d = 11.01 ± 1.541 nm). **(B)** TEM image of DOTA-IO-GUL.

(Gibco®, Life Technologies Korea, Korea) containing 1% (v/v) antibiotic-antimycotic (100×) (Gibco®, Life Technologies Korea, Korea). The LNCaP and PC-3 cell lines were purchased from the Korean Cell Line Bank (KCLB, Seoul, Korea). The LNCaP cell culture was grown in minimum essential medium (MEM) (Gibco®, Life Technologies Korea, Korea) mixed with 10% (v/v) heat-inactivated FBS containing 1% (v/v) antibiotic-antimycotic (100×). The PC-3 cells were cultured in the same medium used for the 22Rv1 cell line.

In vitro competitive cell binding assay

LNCaP and PC-3 cells were used for competition binding analysis as PSMA-positive and PSMA-negative cell lines, respectively. The cells were plated in 24-well plates at approximately 2×10^5 cells/well and incubated for 24 h in a humidified incubator at 37 °C with 5% CO_2 supply. DOTA-IO-GUL was serially diluted in a serum-free cell culture medium containing 0.5% bovine serum albumin. Each 0.5 mL of the diluted DOTA-IO-GUL sample was added to the cells with 1.85 kBq/0.5 mL of ^{125}I labeled (*S*)-2-(3-((*S*)-1-carboxy-5-((4-iodobenzyl)amino)pentyl)ureido)pentanedioic acid (^{125}I-MIP-1072)[50] and incubated for 1 h in a humidified incubator at 37 °C with 5% CO_2. After 1 h, the media were aspirated and the pellet was washed twice by dispersal in fresh assay medium cells. One mL of 1% sodium dodecyl sulfate in phosphate buffered saline was added to each well and gently mixed to

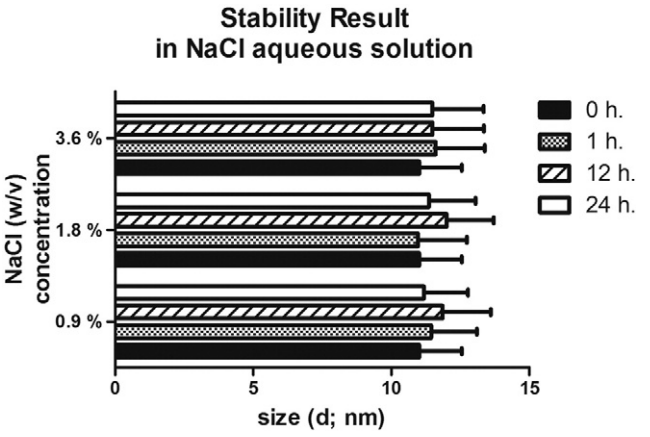

Figure 3. DOTA-IO-GUL stability study in 0.9%, 1.8% and 3.6% NaCl solutions for 1 h, 12 h and 24 h. **(B)** ^{68}Ga-DOTA-IO-GUL stability study in human serum for 2 h at 36.5 °C. **(C)** ^{68}Ga-DOTA-IO-GUL stability study in human serum for 2 h at 36.5 °C.

dissolve cells. The dissolved cells were transferred to 5-mL plastic test tubes. Radioactivity was counted by a gamma scintillation counter.

Establishing a xenograft model

Specific pathogen-free 4-week old male BALB/c nude mice were used for all animal studies. 5×10^6 cells each of the 22Rv1 and PC-3 cell lines in 0.1 mL of RPMI-1640 medium were subcutaneously injected into the left and right flanks of mice, respectively. The xenografted tumors were grown for 2-3 weeks and then the mice were used for *in vivo* imaging studies.

PET imaging study in mouse xenograft model

^{68}Ga-DOTA-IO-GUL in normal saline (10.2 MBq, 100 μL) was injected into the 22Rv1 xenograft mice via the tail vein. After 1 h, images of the mice were obtained by static mode for 10 min under isoflurane anesthesia. These PET images were acquired by 3-dimensional Fourier re-binning using a 2-dimensional ordered-subsets expectation maximization reconstruction algorithm using the MMWKS-Vista software. For each PET scan, 3-dimensional regions of interest (ROI) were drawn over tumors on whole-body axial images. Standardized uptake values (SUV) were obtained using reconstructed data for each PET imaging system.

MRI imaging study in mouse xenograft model

A phantom study was performed to prove the dose-dependent MR signal acquisition. T2-weighted images were obtained using a phantom prepared with PCR tubes containing serially diluted DOTA-IO-GUL (200, 100, 50.0, 25.0, 12.5, 6.25 and 3.13 μM of ferric ion) in agarose solution. For animal MR imaging, 22Rv1 and PC-3 xenografted mice were used. The control MR image was obtained before the DOTA-IO-GUL injection in anesthesia by isoflurane/O_2 (2% isoflurane, 1.0 L/min oxygen). The T2-weighted image was measured in fast spin echo multiple slice (FSEMS) pulse sequence. The retention time was 3000 ms and the effective echo time was 29.0 ms. Echo train length (ETL) was 4, and the average was also 4. The matrix was 192 × 192

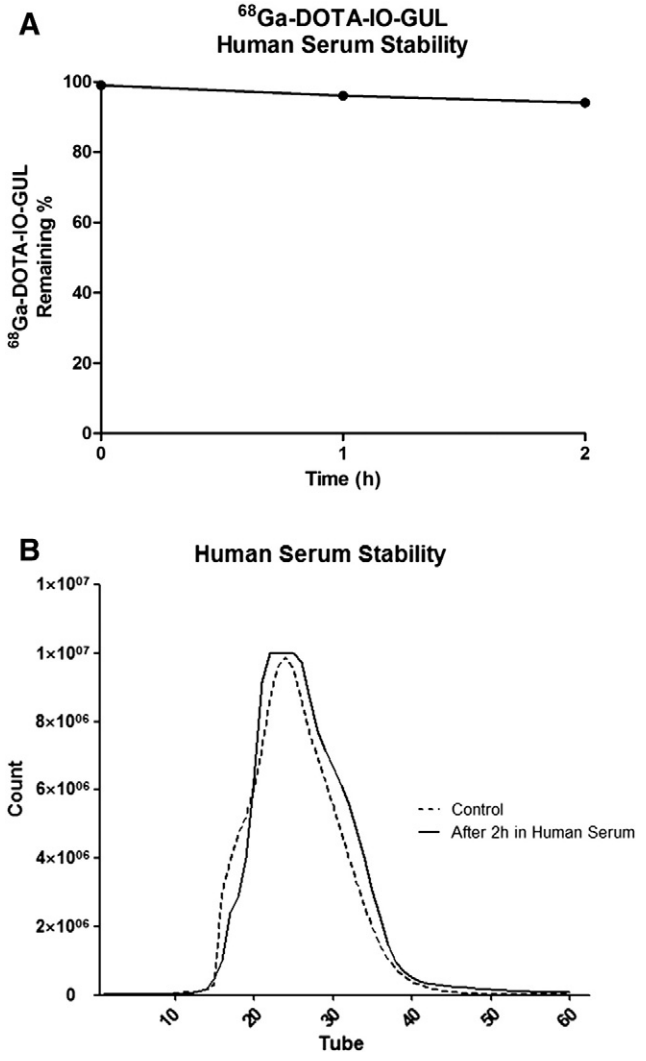

Figure 4. ^{68}Ga-DOTA-IO-GUL stability study in human serum for 2 h at 36.5 °C. **(A)** Radiochemical purity (%) of ^{68}Ga-DOTA-IO-GUL checked by ITLC after incubation in human serum. **(B)** Elution profiles of ^{68}Ga-DOTA-IO-GUL control and 2 h after incubated ^{68}Ga-DOTA-IO-GUL in human serum determined by the Sephacryl® S-500 HR gel filtration chromatography.

and the orientation was coronal. The field of view was 18.0 × 35.0 mm^2. The slices were 15 and slice thickness was 1.00 mm. After completion of the control MR imaging study, DOTA-IO-GUL 200 μM in 0.1 mL normal saline was injected into the tail vein of the mice. After 1 h, the T2-weighted MR image was obtained through the same method as control mice imaging. These MRI results were analyzed using the Sante DICOM viewer program.

Results

Preparation of IO NPs

The specific amphiphiles (*S*)-2-(3-((*S*)-1-carboxy-5-stearamidopentyl)ureido)pentanedioic acid (GUL-SA) and 2,2′,2″,2‴-(2-(4-(3-octadecylthioureido)benzyl)-1,4,7,10-tetraazacyclododecane-1,4,7,10-tetrayl)tetraacetic acid (DOTA-SA) were synthesized by 2- and 1-step reactions with 45% and 36% yields, respectively (supplementary material Schemes S1 and S2). These amphiphiles were used for the encapsulation of IO core. The encapsulated NP DOTA-IO-GUL, a dark brown liquid, was obtained using the schematic method with a final yield if 85% (Figure 1, *A*). The prepared DOTA-IO-GUL has an IO core and a functionalized capsule composed of polysorbate 60, DOTA-SA and GUL-SA (Figure 1, *B*). Polysorbate 60 provides a polyethyleneglycol (PEG) side chain which allows it to escape from the immune system, known as the "stealth effect". The DOTA moiety is used for radiolabeling with metallic a radioisotope (^{68}Ga in this study) and the GUL moiety is used for targeting PSMA. The diameter of DOTA-IO-GUL, measured by dynamic light scattering (DLS), was 11.01 ± 1.541 nm (Figure 2, *A*), which was confirmed by transmission electron microscopy (TEM) imaging (Figure 2, *B*).

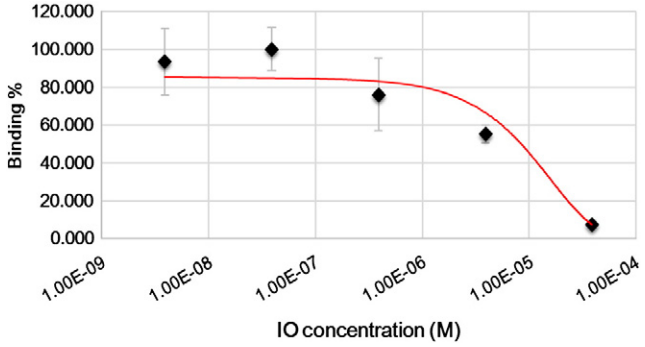

Figure 5. *In vitro* cell binding assay result. Bound radioactivity of ^{125}I-MIP-1072, a PSMA-inhibitor, to the PSMA-positive cells, LNCaP, showed a dose-dependent decrease by addition of DOTA-IO-GUL.

Radiochemistry

The DOTA-IO-GUL was labeled with ^{68}Ga in a sodium acetate buffer (pH 5.6), with over 99% efficiency. According to radio thin layer chromatography (TLC) (ITLC-SG: solid phase, 0.1 M citric acid: mobile phase), ^{68}Ga-DOTA-IO-GUL remained at the origin (R_f = 0.0) and free ^{68}Ga moved with the solvent front line (R_f = 1.0). The medium of the radiolabeled mixture was replaced with distilled water by centrifugal ultrafiltration and then concentrated to 100 μL for the following experiments. The radiochemical purity of the final purified ^{68}Ga-DOTA-IO-GUL was higher than 99% (supplementary material Figure S1).

Stability tests

NPs tend to aggregate in high salt solution which is one of the most common stability problems of NPs. In order to test the stability of DOTA-IO-GUL, it was incubated with various concentrations of NaCl aqueous solutions (0%, 0.9%, 1.8%, and 3.6%) for 24 h. Then the particle sizes of the solutions were measured using dynamic light scattering (DLS) to check for aggregation at 1, 12 and 24 h post-incubation (Figure 3). The results revealed that DOTA-IO-GUL size did not show any significant changes in the above conditions. This

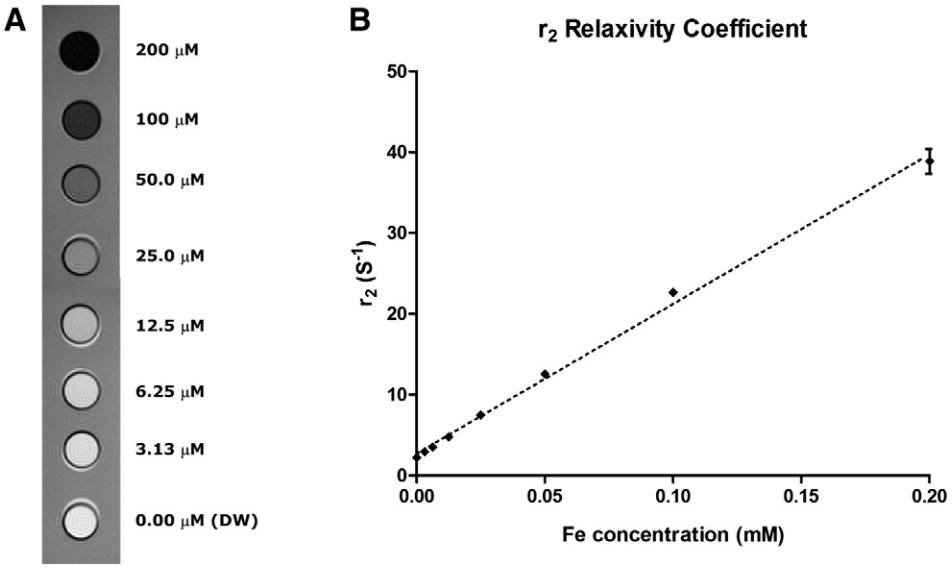

Figure 6. MRI phantom study for the determination of DOTA-IO-GUL injection concentration. **(A)** MR image was obtained from serially diluted DOTA-IO-GUL from 200 μM Fe^{3+} concentration. **(B)** Calculation of r_2 relaxivity coefficient value of DOTA-IO-GUL ($y = 185.13 x + 2.6898$; $R^2 = 0.9968$).

demonstrated that the prepared NP, DOTA-IO-GUL, is stable in salt solutions that are even 4-times more concentrated than physiological condition.

After being labeled with ^{68}Ga, the ^{68}Ga-DOTA-IO-GUL was incubated in human serum at 37 °C with shaking. The stability was checked by radio TLC after 2 h of incubation as mentioned in the experimental section, and found to have 94% stability (Figure 4, *A*, supplementary material Figure S1c). Additionally, we compared the elution profiles of ^{68}Ga-DOTA-IO-GUL before and after 2 h incubation in human serum using Sephacryl® S-500 HR gel filtration chromatography (Figure 4, *A*). The result showed no significant change of elution profile, which proved that the ^{68}Ga-DOTA-IO-GUL nanoparticle was stable in human serum at 36.5 °C.

According to these *in vitro* experimental results, we found that ^{68}Ga-DOTA-IO-GUL is stable enough to be used as a PET probe.

Competitive binding study using a PSMA-positive cell line

Specific binding of DOTA-IO-GUL to PSMA-positive cells was confirmed by an *in vitro* competitive binding study. A previously reported PSMA-imaging agent, ^{123}I-MIP-1072, was used as a radiolabeled ligand.[50,51]. The PSMA-positive human prostate cancer cell line, LNCaP, was incubated with ^{125}I-MIP-1072 and various concentration of DOTA-IO-GUL at room temperature for 1 h. After the aspiration of unbound fractions, the cell-bound radioactivities were measured. A binding curve with dose-dependent blocking was obtained (Figure 5), which proved the specific binding of DOTA-IO-GUL to PSMA-positive cells.

In vivo imaging study using a xenograft model

MR imaging of a phantom composed of serially diluted aqueous solutions of 200 μM DOTA-IO-GUL demonstrated the linearity of T2-weighted MR signal with IO concentrations (Figure 6).

For *in vivo* imaging studies, a BALB/c mouse model having prostate cancer xenografts of the PSMA-positive cell line (22Rv1) and PSMA-negative cell line (PC-3) at the left and right flank, respectively, was established. Both of the 22Rv1 and PC-3 tumor MR images taken before administration of NOTA-IO-GUL were shown to be white masses (Figure 7, *A*). However, decreased MR signals (as block dots) were found with the 22Rv1 tumor, representing increased uptake of IO NPs after an injection of DOTA-IO-GUL, while the PC-3 tumor did not show any change. This result demonstrated that DOTA-IO-GUL was only taken up by the PSMA-positive 22Rv1 tumor and not by the PSMA-negative PC-3 tumor (Figure 7, *B*). However, this MR imaging study could not provide quantitative information on tumor uptake.

PET images were obtained 1 h post-injection of ^{68}Ga-DOTA-IO-GUL through the tail vein, and the uptake of ^{68}Ga-DOTA-IO-GUL was found only in the 22Rv1 tumor, which was consistent with the MR imaging study (Figure 8, *A*). However, the resolution of PET images was much lower than MR images. The obviously dotted MR images showed localized distribution in the tumor with higher resolution than PET. On the other hand, the PSMA-specific uptake could be proved by a blocking study *in vivo* using PET imaging. A known PSMA-specific small molecule, MIP-1072, was co-injected with ^{68}Ga-DOTA-IO-GUL through the tail vein, and it was found that ^{68}Ga-DOTA-IO-GUL uptake was blocked (Figure 8, *B*). The specific uptake of ^{68}Ga-DOTA-IO-GUL by the PSMA-positive tumor was proven by these results.

In addition, the PET imaging study could be used for the quantification of tumor uptakes. The amount of the injected ^{68}Ga-DOTA-IO-GUL was 1.544 μg. The standard uptake value (SUV) of the 22Rv1 tumor was calculated as 2.385 from the PET image, and the amount of IO in the 22Rv1 tumor was calculated to be 0.0825 μg.

Based on these imaging studies, it was demonstrated that MR images show a higher resolution of tumor uptake, and PET

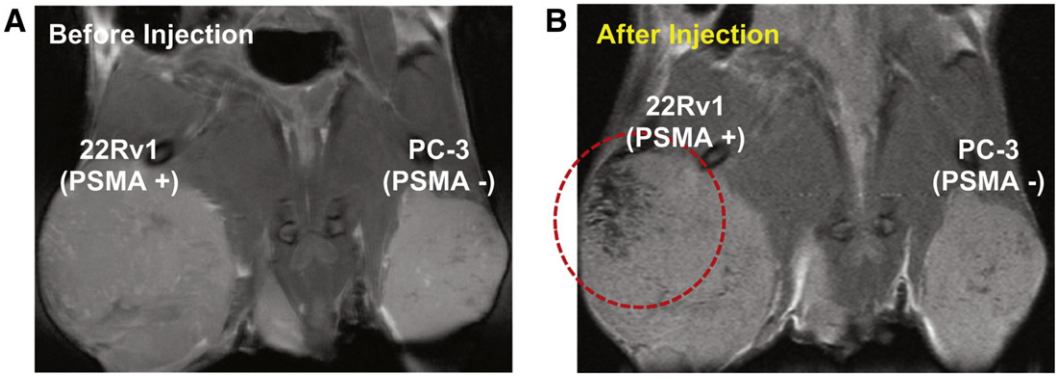

Figure 7. *In vivo* micro MRI image results. **(A)** Before injection, control image; **(B)** after injection of DOTA-IO-GUL (0.1 mL, 0.2 mM) through the tail vein (1 h). Left tumor is PSMA positive (22Rv1) and right tumor is PSMA-negative (PC-3). Red circle demonstrates the selective uptake of DOTA-IO-GUL to the positive tumor (49.1 Fe ng/g).

images can confirm the specific uptake and provide quantitative results of tumor uptake.

Discussion

PET/MR dual imaging is an attractive imaging tool for the next generation of molecular imaging field. MR imaging can provide high-resolution anatomical imaging, while PET imaging can provide specific binding and quantitative information. In addition, PET can provide images with high sensitivity to microdoses of radioisotopes. Development of an efficient and reliable PET/MR dual-imaging probe is essential to actualize the PET/MR instrument's powerful application.

IO-based nanoparticles are one of the best options for a PET/MR dual imaging probe, especially because the basis of IO is iron which exists in abundantly in the human body particularly in blood. Thus, IO NPs are known to be less toxic than a gadolinium (Gd)-based MR contrast agents.[52] In the present study, DOTA-IO-GUL was prepared by the encapsulation of oleic acid-coated IO NPs using special amphiphiles such as GUL-SA, NOTA-SA and polysorbate 60. GUL-SA and NOTA-SA were easily prepared by organic synthesis.

GUL is a specific PSMA-targeting moiety. Prostate cancer is now one of the most rapidly increasing types of cancer worldwide. Thus the necessity of dual-modal imaging probes like DOTA-IO-GUL for early and accurate diagnosis of prostate cancer is extremely high.

The uptake of NPs by tumors is often associated with the enhanced permeability and retention (EPR) effect, which can occur with nanoparticles to any kind of tumors, non-specifically.[53-55] However, in this study, we used a PSMA-positive and PSMA-negative tumor xenografted mouse model to prove the specificity. Uptake of DOTA-IO-GUL was revealed only in the PSMA-positive tumor by both PET and MR imaging. If the DOTA-IO-GUL uptake by the tumor was by the EPR effect, the uptake might be exhibited in both the PSMA-positive and negative tumors. We also proved by PET imaging that the uptake of DOTA-IO-GUL could be blocked by a PSMA-binding agent, which definitely demonstrated that the uptake was specific but not EPR effect.

In this experiment, we could distinguish the specific uptake of DOTA-IO-GUL to the PSMA-positive tumor by MR imaging by using a mouse model xenografted with both PSMA-positive and negative tumors, and MR images were obtained both before and after administration of DOTA-IO-GUL. However, in clinical settings, MR imaging would produce gray tumor images which would make it almost impossible to distinguish whether it is positive or not. Thus, the cancer specificity can be provided only by PET imaging, but not by MR imaging in clinical practice.

Another important point to consider about the PET/MR dual-imaging agent is the different sensitivities of PET and MRI. One of the most important advantages of PET is its high sensitivity, thus microdosing of the contrast agent is enough to obtain high quality imaging.[56] On the other hand, due to its low sensitivity, a much higher dose of contrast agent is required for MR imaging than PET. In order to solve this problem, microdose of ^{68}Ga-DOTA-IO-GUL having a high enough radioactivity (10.2 MBq) was used for PET imaging and cold DOTA-IO-GUL having enough concentration for MRI contrast agent (0.2 M) was used for MR imaging in this study. Thus, we could obtain both PET and MR images successfully.

Although PET can provide us with highly specific images, it tends to produce images with low resolution. Positron emitters can travel a few millimeters before annihilation occurs, which is a cause of decreasing resolution. In addition, the partial volume effect also affects resolution especially in small objects. These are intrinsic problems of PET imaging, which can be compensated by a simultaneous MRI or CT.

Furthermore, DOTA-IO-GUL can be labeled not only with ^{68}Ga but also with therapeutic beta emitters such as ^{90}Y or ^{177}Lu which have low penetration and high cytotoxic effects. Therefore, it has possibility of being used for theranostic application in the future.

In summary, we prepared a PSMA-targeting IO NP as a PET/MR dual-imaging probe by a straightforward and reliable method: encapsulation of NPs with specially prepared amphiphiles. Additionally, this method can be easily and widely used for many other diseases and targeting biomarkers by targeting-moiety introduced specific amphiphiles.

The prepared NP, ^{68}Ga-DOTA-IO-GUL, showed high radiolabeling efficiency at pH 5.6 and was stable in high-salt concentration. The specific binding of ^{68}Ga-DOTA-IO-GUL to

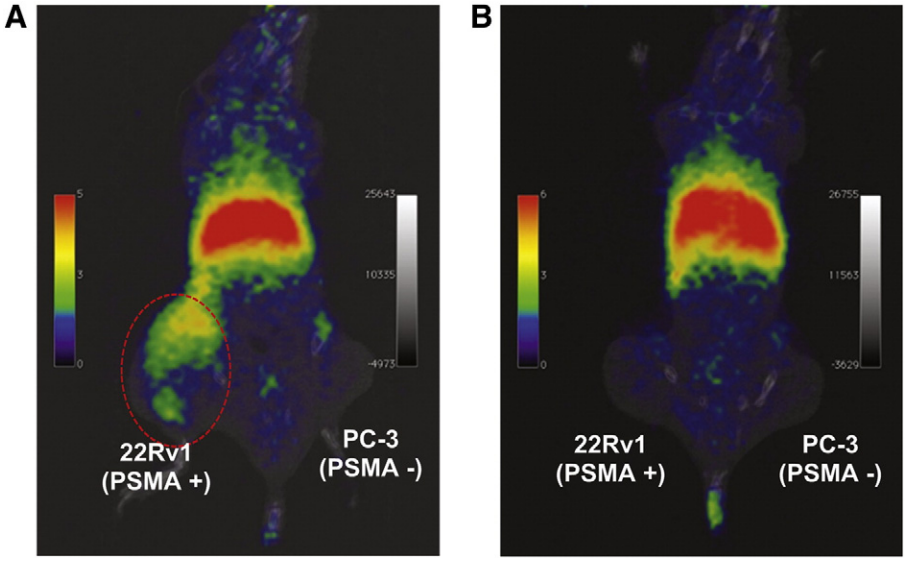

Figure 8. *In vivo* PET result. **(A)** PSMA-selective uptake result in micro PET imaging. (SUV_{mean} = 0.668) ^{68}Ga-DOTA-IO-GUL (10.2 MBq, 0.1 mL) tail vein injection after 1 h imaging. Left tumor is PSMA-positive (22Rv1) and right tumor is PSMA-negative (PC-3). **(B)** Blocking study result with co-injection of MIP-1072 (50 mg/kg).

PSMA-positive cells was confirmed *in vitro* and *in vivo*. PET/MR dual images were successfully obtained by using an adequate amount of radioactivity and cold NPs to adjust the sensitivity of each modality. MR images showed a high uptake of the NP by the PSMA-positive tumor with high resolution, but were limited in providing quantitative information. PET images also showed specific uptake by the PSMA-positive tumor, and furthermore provided quantitative information. With this information, the amount of IO NP accumulated in the tumor could be calculated. However, the resolution of PET images was lower than the MR images. In conclusion, ^{68}Ga-DOTA-IO-GUL has shown to be a promising dual-modal agent for the imaging of prostate cancer, with the complementary effects of each imaging modality.

References

1. Hofmann M, Pichler B, Schölkopf B, Beyer T. Towards quantitative PET/MRI: a review of MR-based attenuation correction techniques. *Eur J Nucl Med Mol Imaging* 2009;**36**:93-104.
2. Schulz V, Torres-Espallardo I, Renisch S, Hu Z, Ojha N, Börnert P, et al. Automatic, three-segment, MR-based attenuation correction for whole-body PET/MR data. *Eur J Nucl Med Mol Imaging* 2011;**38**:138-52.
3. Zhou J, Yu M, Sun Y, Zhang X, Zhu X, Wu Z, et al. Fluorine-18-labeled Gd3þ/Yb3þ/Er3þ co-doped NaYF4 nanophosphors for multimodality PET/MR/UCL imaging. *Biomaterials* 2011;**32**:1148-56.
4. Delso G, Fürst S, Jakoby B, Ladebeck R, Ganter C, Nekolla SG, et al. Performance measurements of the Siemens mMR integrated whole-body PET/MR scanner. *J Nucl Med* 2011;**52**:1914-22.
5. Aryal S, Key J, Stigliano C, Landis MD, Lee DY, Decuzzi P. Positron emitting magnetic nanoconstructs for PET/MR imaging. *Small* 2014;**10**:2688-96.
6. Schlyer D, Ravindranath B. *Dual-Modality Preclinical PET/MRI Instrumentation*. Molecular Imaging of Small Animals. Springer; 2014409-45.
7. Drzezga A, Souvatzoglou M, Eiber M, Beer AJ, Fürst S, Martinez-Möller A, et al. First clinical experience with integrated whole-body PET/MR: comparison to PET/CT in patients with oncologic diagnoses. *J Nucl Med* 2012;**53**:845-55.
8. Kim JS, Kim Y-H, Kim JH, Kang KW, Tae EL, Youn H, et al. Development and *in vivo* imaging of a PET/MRI nanoprobe with enhanced NIR fluorescence by dye encapsulation. *Nanomedicine* 2012;**7**:219-29.
9. Lee H-Y, Li Z, Chen K, Hsu AR, Xu C, Xie J, et al. PET/MRI dual-modality tumor imaging using arginine-glycine-aspartic (RGD)–conjugated radiolabeled iron oxide nanoparticles. *J Nucl Med* 2008;**49**:1371-9.
10. Thorek DL, Ulmert D, Diop N-FM, Lupu ME, Doran MG, Huang R, et al. Non-invasive mapping of deep-tissue lymph nodes in live animals using a multimodal PET/MRI nanoparticle. *Nat Commun* 2014;**5**:3097-105, http://dx.doi.org/10.1038/ncomms4097.
11. Yang X, Hong H, Grailer JJ, Rowland IJ, Javadi A, Hurley SA, et al. cRGD-functionalized, DOX-conjugated, and ^{64}Cu-labeled superparamagnetic iron oxide nanoparticles for targeted anticancer drug delivery and PET/MR imaging. *Biomaterials* 2011;**32**:4151-60.
12. Choi JS, Park JC, Nah H, Woo S, Oh J, Kim KM, et al. A hybrid nanoparticle probe for dual-modality positron emission tomography and magnetic resonance imaging. *Angew Chem Int Ed* 2008;**47**:6259-62.
13. Tsoukalas C, Laurent G, Sánchez GJ, Tsotakos T, Bazzi R, Stellas D, et al. Initial *in vitro* and *in vivo* assessment of Au@ DTDTPA-RGD nanoparticles for Gd-MRI and ^{68}Ga-PET dual modality imaging. *EJNMMI Physic* 2015;**2**:A89.
14. Lewis CM, Graves SA, Hernandez R, Valdovinos HF, Barnhart TE, Cai W, et al. ^{52}Mn production for PET/MRI tracking of human stem cells expressing divalent metal transporter 1 (DMT1). *Theranostics* 2015;**5**:227-39.
15. Binderup T, Lobatto M, Perez-Medina C, Giesen L, Robson P, Calcagno C, et al. PET/MRI to predict and quantify the uptake of ^{89}Zr-labeled nanoparticles in the aortic wall of atherosclerotic rabbits. *Paper presented at: Society of Nuclear Medicine Annual Meeting*; 2014. p. 186. [Abstracts].
16. Tu C, Ng TS, Jacobs RE, Louie AY. Multimodality PET/MRI agents targeted to activated macrophages. *J Biol Inorg Chem* 2014;**19**:247-58.
17. Truillet C, Lux F, Bouziotis P, Martini M, Tsoukalas C, Sancey L, et al. Development of ^{68}Ga/Gd^{3+} multimodal nanoparticles for PET/MRI dual imaging for tumor detection. *J Nucl Med* 2015;**56**(supplement):273.

18. Nahrendorf M, Zhang H, Hembrador S, Panizzi P, Sosnovik DE, Aikawa E, et al. Nanoparticle PET-CT imaging of macrophages in inflammatory atherosclerosis. *Circulation* 2008;**117**:379-87.
19. Yan L, Zhang J, Lee CS, Chen X. Micro- and nanotechnologies for intracellular delivery. *Small* 2014;**10**:4487-504.
20. Narayanan R, El-Sayed MA. Catalysis with transition metal nanoparticles in colloidal solution: nanoparticle shape dependence and stability. *J Phys Chem B* 2005;**109**:12663-76.
21. Knauert ST, Douglas JF, Starr FW. The effect of nanoparticle shape on polymer-nanocomposite rheology and tensile strength. *J Polym Sci B* 2007;**45**:1882-97.
22. Li N, Binder WH. Click-chemistry for nanoparticle-modification. *J Mater Chem* 2011;**21**:16717-34.
23. Fang F, Zhao D, Li B, Zhang Z, Zhang J, Shen D. The enhancement of ZnO nanowalls photoconductivity induced by CdS nanoparticle modification. *Appl Phys Lett* 2008;**93**:233115.
24. Lee YK, Jeong JM, Hoigebazar L, Yang BY, Lee YS, Lee BC, et al. Nanoparticles modified by encapsulation of ligands with a long alkyl chain to affect multispecific and multimodal imaging. *J Nucl Med* 2012;**53**:1462-70.
25. Yang BY, Moon SH, Seelam SR, Jeon MJ, Lee YS, Lee DS, et al. Development of a multimodal imaging probe by encapsulating iron oxide nanoparticles with functionalized amphiphiles for lymph node imaging. *Nanomedicine (Lond)* 2015;**10**:1899-910.
26. Lee DS, Im HJ, Lee YS. Radionanomedicine: widened perspectives of molecular theragnosis. *Nanomedicine* 2015;**11**:795-810.
27. Seo HJ, Nam SH, Im H-J, Park J-Y, Lee JY, Yoo B, et al. Rapid hepatobiliary excretion of micelle-encapsulated/radiolabeled upconverting nanoparticles as an integrated form. *Sci Report* 2015;**5**:15685.
28. Babes L, Denizot Bt, Tanguy G, Le Jeune JJ, Jallet P. Synthesis of iron oxide nanoparticles used as MRI contrast agents: a parametric study. *J Colloid Interface Sci* 1999;**212**:474-82.
29. Chertok B, Moffat BA, David AE, Yu F, Bergemann C, Ross BD, et al. Iron oxide nanoparticles as a drug delivery vehicle for MRI monitored magnetic targeting of brain tumors. *Biomaterials* 2008;**29**:487-96.
30. Higuchi T, Anton M, Dumler K, Seidl S, Pelisek J, Saraste A, et al. Combined reporter gene PET and iron oxide MRI for monitoring survival and localization of transplanted cells in the rat heart. *J Nucl Med* 2009;**50**:1088-94.
31. Rosen JE, Chan L, Shieh D-B, Gu FX. Iron oxide nanoparticles for targeted cancer imaging and diagnostics. *Nanomedicine: NBM* 2012;**8**:275-90.
32. Schwarz S, Wong JE, Bornemann J, Hodenius M, Himmelreich U, Richtering W, et al. Polyelectrolyte coating of iron oxide nanoparticles for MRI-based cell tracking. *Nanomedicine: NBM* 2012;**8**:682-91.
33. Jon S, Lee H, Yu MK, Jeong YY. Multifunctional Superparamagnetic Iron Oxide Nanoparticles (SPION) for cancer imaging and therapy. *Nanomedicine: NBM* 2007;**3**:348.
34. Xie J, Chen K, Huang J, Lee S, Wang J, Gao J, et al. PET/NIRF/MRI triple functional iron oxide nanoparticles. *Biomaterials* 2010;**31**:3016-22.
35. Zhernosekov KP, Filosofov DV, Baum RP, Aschoff P, Bihl H, Razbash AA, et al. Processing of generator-produced ^{68}Ga for medical application. *J Nucl Med* 2007;**48**:1741-8.
36. Meyer GJ, Macke H, Schuhmacher J, Knapp WH, Hofmann M. ^{68}Ga-labelled DOTA-derivatised peptide ligands. *Eur J Nucl Med Mol Imaging* 2004;**31**:1097-104.
37. Shetty D, Lee YS, Jeong JM. ^{68}Ga-labeled radiopharmaceuticals for positron emission tomography. *Nucl Med Mol Imaging* 2010;**44**:233-40.
38. Jeong JM, Hong MK, Chang YS, Lee YS, Kim YJ, Cheon GJ, et al. Preparation of a promising angiogenesis PET imaging agent: ^{68}Ga-labeled c(RGDyK)-isothiocyanatobenzyl-1,4,7-triazacyclononane-1,4,7-triacetic acid and feasibility studies in mice. *J Nucl Med* 2008;**49**:830-6.
39. Hoigebazar L, Jeong JM, Choi SY, Choi JY, Shetty D, Lee YS, et al. Synthesis and characterization of nitroimidazole derivatives for ^{68}Ga-labeling and testing in tumor xenografted mice. *J Med Chem* 2010;**53**:6378-85.
40. Breeman WA, de Blois E, Sze Chan H, Konijnenberg M, Kwekkeboom DJ, Krenning EP. ^{68}Ga-labeled DOTA-peptides and ^{68}Ga-labeled radiopharmaceuticals for positron emission tomography: current status of research, clinical applications, and future perspectives. *Semin Nucl Med* 2011;**41**:314-21.
41. Siegel R, Ma J, Zou Z, Jemal A. Cancer statistics, 2014. *CA Cancer J Clin* 2014;**64**:9-29.
42. Ferlay J, Soerjomataram I, Dikshit R, Eser S, Mathers C, Rebelo M, et al. Cancer incidence and mortality worldwide: sources, methods and major patterns in GLOBOCAN 2012. *Int J Cancer* 2015;**136**:E359-86.
43. Trover JK, Beckett ML, Wright GL. Detection and characterization of the prostate-specific membrane antigen (PSMA) in tissue extracts and body fluids. *Int J Cancer* 1995;**62**:552-8.
44. Eder M, Eisenhut M, Babich J, Haberkorn U. PSMA as a target for radiolabelled small molecules. *Eur J Nucl Med Mol Imaging* 2013;**40**:819-23.
45. Yu MK, Kim D, Lee IH, So JS, Jeong YY, Jon S. Image-guided prostate cancer therapy using aptamer-functionalized thermally cross-linked superparamagnetic iron oxide nanoparticles. *Small* 2011;**7**:2241-9.
46. Kratochwil C, Giesel FL, Leotta K, Eder M, Hoppe-Tichy T, Youssoufian H, et al. PMPA for nephroprotection in PSMA-targeted radionuclide therapy of prostate cancer. *J Nucl Med* 2015;**56**:293-8.
47. Chen Z, Penet M-F, Nimmagadda S, Li C, Banerjee SR, Winnard PT, et al. PSMA-targeted theranostic nanoplex for prostate cancer therapy. *ACS Nano* 2012;**6**:7752-62.
48. Schipper ML, Iyer G, Koh AL, Cheng Z, Ebenstein Y, Aharoni A, et al. Particle size, surface coating, and PEGylation influence the biodistribution of quantum dots in living mice. *Small* 2009;**5**:126-34.
49. Chen Y, Foss CA, Byun Y, Nimmagadda S, Pullambhatla M, Fox JJ, et al. Radiohalogenated prostate-specific membrane antigen (PSMA)-based ureas as imaging agents for prostate cancer. *J Med Chem* 2008;**51**:7933-43.
50. Maresca K, Hillier S, Femia F, Keith D, Barone C, Joyal J, et al. A series of halogenated heterodimeric inhibitors of prostate specific membrane antigen (PSMA) as radiolabeled probes for targeting prostate cancer. *J Med Chem* 2008;**52**:347-57.
51. Hillier SM, Kern AM, Maresca KP, Marquis JC, Eckelman WC, Joyal JL, et al. ^{123}I-MIP-1072, a small-molecule inhibitor of prostate-specific membrane antigen, is effective at monitoring tumor response to taxane therapy. *J Nucl Med* 2011;**52**:1087-93.
52. Cacheris WP, Quay SC, Rocklage SM. The relationship between thermodynamics and the toxicity of gadolinium complexes. *Magn Reson Imaging* 1990;**8**:467-81.
53. Maeda H. The enhanced permeability and retention (EPR) effect in tumor vasculature: the key role of tumor-selective macromolecular drug targeting. *Adv Enzyme Regul* 2001;**41**:189-207.
54. Maeda H, Sawa T, Konno T. Mechanism of tumor-targeted delivery of macromolecular drugs, including the EPR effect in solid tumor and clinical overview of the prototype polymeric drug SMANCS. *J Control Release* 2001;**74**:47-61.
55. Maeda H, Bharate G, Daruwalla J. Polymeric drugs for efficient tumor-targeted drug delivery based on EPR-effect. *Eur J Pharm Biopharm* 2009;**71**:409-19.
56. Bergström M, Grahnen A, Långström B. Positron emission tomography microdosing: a new concept with application in tracer and early clinical drug development. *Eur J Clin Pharmacol* 2003;**59**:357-66.